Dear Author,

Here are the proofs of your article.

- You can submit your corrections **online**, via **e-mail** or by **fax**.
- For **online** submission please insert your corrections in the online correction form. Always indicate the line number to which the correction refers.
- You can also insert your corrections in the proof PDF and **email** the annotated PDF.
- For fax submission, please ensure that your corrections are clearly legible. Use a fine black pen and write the correction in the margin, not too close to the edge of the page.
- Remember to note the **journal title**, **article number**, and **your name** when sending your response via e-mail or fax.
- **Check** the metadata sheet to make sure that the header information, especially author names and the corresponding affiliations are correctly shown.
- **Check** the questions that may have arisen during copy editing and insert your answers/ corrections.
- **Check** that the text is complete and that all figures, tables and their legends are included. Also check the accuracy of special characters, equations, and electronic supplementary material if applicable. If necessary refer to the *Edited manuscript*.
- The publication of inaccurate data such as dosages and units can have serious consequences. Please take particular care that all such details are correct.
- Please **do not** make changes that involve only matters of style. We have generally introduced forms that follow the journal's style.
  Substantial changes in content, e.g., new results, corrected values, title and authorship are not allowed without the approval of the responsible editor. In such a case, please contact the Editorial Office and return his/her consent together with the proof.
- If we do not receive your corrections **within 48 hours**, we will send you a reminder.
- Your article will be published **Online First** approximately one week after receipt of your corrected proofs. This is the **official first publication** citable with the DOI. **Further changes are, therefore, not possible.**
- The **printed version** will follow in a forthcoming issue.

Please note

After online publication, subscribers (personal/institutional) to this journal will have access to the complete article via the DOI using the URL: http://dx.doi.org/[DOI].
If you would like to know when your article has been published online, take advantage of our free alert service. For registration and further information go to: http://www.link.springer.com.

Due to the electronic nature of the procedure, the manuscript and the original figures will only be returned to you on special request. When you return your corrections, please inform us if you would like to have these documents returned.

Metadata of the article that will be visualized in OnlineFirst

ArticleTitle	Bifurcation and Chaos in indirect field-oriented controlled induction motor drive system	
Article Sub-Title		
Article CopyRight	The Author(s), under exclusive licence to Società Italiana di Fisica and Springer-Verlag GmbH Germany, part of Springer Nature (This will be the copyright line in the final PDF)	
Journal Name	The European Physical Journal Plus	

Corresponding Author	Family Name	**Hunaish**
	Particle	
	Given Name	**Ahmed Sadeq**
	Suffix	
	Division	Electrical Engineering Department
	Organization	University of Basrah
	Address	Basrah, Iraq
	Phone	
	Fax	
	Email	ahm782013@gmail.com
	URL	
	ORCID	http://orcid.org/0000-0001-8317-8581
Author	Family Name	**Tahir**
	Particle	
	Given Name	**Fadhil Rahma**
	Suffix	
	Division	Electrical Engineering Department
	Organization	University of Basrah
	Address	Basrah, Iraq
	Phone	
	Fax	
	Email	fadhilrahma.creative@gmail.com
	URL	
	ORCID	

	Received	14 August 2020
Schedule	Revised	
	Accepted	31 March 2021

Abstract

In this paper, the higher-order three-phase indirect field-oriented controlled (IFOC) induction motor is modeled in synchronous reference frame. The IFOC induction motor is analyzed numerically to investigate the system behavior due to control parameters change. The slip speed compensator, integral, and proportional gains variations of the speed loop controller are used to confirm the system dynamics. The simulation results show that the chaos behavior is noted in small region of the slip speed compensator gain which is difficult to be observed through the dominant limit cycles and fixed-point solutions. The effects of the integral and proportional gains change on the system dynamic are verified. Also, the system exhibits period-doubling bifurcation (period-2, period-4, period-8, and period-16) route to chaos. The bifurcation diagram and Lyapunov exponent spectrum assign these situations. The phase portrait and time response results are also presented. The system has multistability and coexistence of different attractors for the same system parameters as represented in the basins of attractions plots.

Footnote Information

Metadata of the article that will be visualized in OnlineAlone

Eur. Phys. J. Plus _####################_
https://doi.org/10.1140/epjp/s13360-021-01389-w

THE EUROPEAN PHYSICAL JOURNAL PLUS

Regular Article

Bifurcation and Chaos in indirect field-oriented controlled induction motor drive system

Ahmed Sadeq Hunaish[a], **Fadhil Rahma Tahir**[b]

Electrical Engineering Department, University of Basrah, Basrah, Iraq

Received: 14 August 2020 / Accepted: 31 March 2021

Abstract In this paper, the higher-order three-phase indirect field-oriented controlled (IFOC) induction motor is modeled in synchronous reference frame. The IFOC induction motor is analyzed numerically to investigate the system behavior due to control parameters change. The slip speed compensator, integral, and proportional gains variations of the speed loop controller are used to confirm the system dynamics. The simulation results show that the 1
chaos behavior is noted in small region of the slip speed compensator gain which is difficult to be observed through the dominant limit cycles and fixed-point solutions. The effects of the integral and proportional gains change on the system dynamic are verified. Also, the system exhibits period-doubling bifurcation (period-2, period-4, period-8, and period-16) route to chaos. The bifurcation diagram and Lyapunov exponent spectrum assign these situations. The phase portrait and time response results are also presented. The system has multistability and coexistence of different attractors for the same system parameters as represented in the basins of attractions plots. 2

1 Introduction

3

Indirect field-oriented controlled (IFOC) [1–6] induction motor (IM) is generally utilized in industrial applications for its high torque performance. The parameters of motor may be changed due to aging and environmental conditions, temperature changes and levels of saturation of IM which maybe lead to the variation of the dynamic and the steady state of the drive system [7]. Also, estimation errors diverge these parameters from its real value [8]. In Ref. [9] and Ref. [10], the PI speed controller was tuned in order to prevent the occurrence of saddle-node bifurcation (SNB) and Hopf bifurcation (HB) in IFOC induction motor. In Ref.[11], the PI speed controller was also tuned theoretically to avoid HB, and the results were validated with some simulation proof. The occurrence of co-dimension-two bifurcation phenomena, such as a Bogdanov–Takens bifurcation (BTB) as well as HB, was provided in [12]. Zero Hopf bifurcation (ZHB) was found in [13] which depends on the PI speed controller gain. HB occurrence was proved [14]; they used time-delayed state feedback criterion to avoid HB which was validated numerically. The speed chaotification was confirmed by both

[a] e-mail: ahm782013@gmail.com (corresponding author)
[b] e-mail: fadhilrahma.creative@gmail.com

simulation and experimental results for periodic speed command by tuning the gain of the compensator for the resistance change due to prolonged operation [15]. By using numerical analysis in [16], a SNB was observed at underestimation of rotor resistance; besides, effect of load change on HB was studied where BTB and ZHB phenomenon were also noted with variations of PI speed loop gain. Simulation and experiment results (for SNB and HB) were also offered.

In the studies [9–14], with ignoring stator current dynamics and less comprehensive loading status, lower-order IM model was relied on. The results in the studies [9–14,16] showed that the general behavior of the system with fixed speed command is the occurrence of the limit cycles (SNB, HB, BTB, and ZHB) in addition to the fixed point. Reference [15] used periodic speed command with and without dc speed offset only to prove the chaotic case, but they did not use fixed speed command, while the fixed speed command is used widely in the industrial applications. The chaotic phenomenon for fixed speed command in dynamics of system was not shown in Refs. [9–14].

In this paper, a bifurcation study on PI-controlled IFOC induction motor is achieved by using a full-order IM model that closes the shortages introduced earlier. Bifurcation situations of IFOCIM are calculated based on linearized model of IFOCIM near the equilibrium point. A numerical analysis is used to investigate period-doubling bifurcation and chaos phenomena with loading condition. The rest of paper is divided into three sections: Sect. 2 deals with IFOCIM system modeling. The scheme of IFOCIM system is introduced, and a mathematical model is derived to investigate the system dynamics. The obtained IFOCIM model consists of eight nonlinear first-order differential equations. Section 3 includes the dynamical analysis of the system. The bifurcation diagrams of the speed of the motor supported with Lyapunov exponent spectrums for a certain ranges of the slip speed compensator gain (α) and PI speed integral gain are plotted by using computer simulation to reveal the period-doubling route to chaos. 2D bifurcation diagram of the speed of the motor due to change of PI speed proportional and integral gains is obtained. The period-doubling route to chaos is indicated in the bifurcation diagrams. Finally, conclusion is provided in Sect. 4.

2 Model of IFOCIM drive system

The general closed-loop control diagram of IFOCIM drive is shown in Fig. 1. The speed and flux signals are fed internally, and the direct (d) and quadrature (q) axes current references (i_{ds} and i_{qs}) are produced from the flux and speed PI controllers. The inverter output is applied to IM, while the controller feedback signals are the currents and voltages of the induction motor stator. The synchronous $d-q$ reference frame model of a squirrel-cage induction motor can be stated according to [3], to have the following full order IM dynamic system:

$$\frac{\mathrm{d}i_{ds}}{\mathrm{d}t} = -\gamma i_{ds} + \omega_e i_{qs} + \zeta\beta\psi_{dr} + \beta\omega_r\psi_{qr} + \frac{v_{ds}}{\sigma L_s} \tag{1}$$

$$\frac{\mathrm{d}i_{qs}}{\mathrm{d}t} = -\omega_e i_{ds} - \gamma i_{qs} - \beta\omega_r\psi_{dr} + \zeta\beta\psi_{qr} + \frac{v_{qs}}{\sigma L_s} \tag{2}$$

$$\frac{\mathrm{d}\psi_{dr}}{\mathrm{d}t} = \zeta L_m i_{ds} - \zeta\psi_{dr} + (\omega_e - \omega_r)\,\psi_{qr} \tag{3}$$

$$\frac{\mathrm{d}\psi_{qr}}{\mathrm{d}t} = \zeta L_m i_{qs} - (\omega_e - \omega_r)\,\psi_{dr} - \zeta\psi_{qr} \tag{4}$$

Journal: Article No.: 1389 TYPESET DISK LE CP Disp.:2021/4/3 Pages: 13 Layout: Small

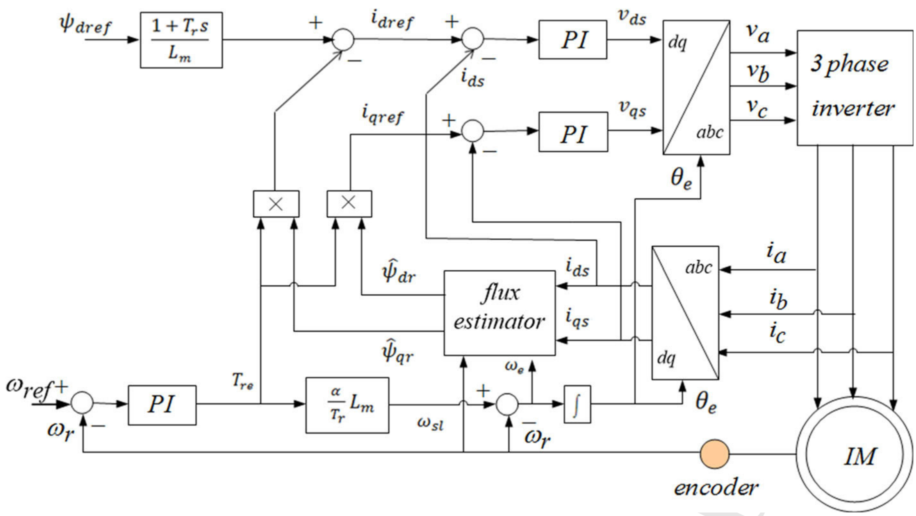

Fig. 1 IFOCIM drive system scheme

Table 1 System parameters definitions

Parameter	Definition	Parameter	Definition
R_s	Stator resistance	P	Number of poles
L_s	Stator inductance	J	Rotor inertia
R_r	Rotor resistance	B_m	Viscous friction coefficient
L_r	Rotor inductance	T_r	Rotor time constant
L_m	Mutual inductance	T_l	Load torque
ω_r	Rotor speed	ω_{ref}	Speed reference

$$\frac{d\omega_r}{dt} = \frac{P}{2J}\left[\frac{3}{2}\frac{P}{2}\frac{L_m}{L_s}\left(\psi_{dr} i_{qs} - \psi_{qr} i_{ds}\right) - T_L - \frac{2}{P} B_m \omega_r\right] \tag{5}$$

where v_{ds}, v_{qs}, ψ_{dr}, and ψ_{qr} are the stator voltage and the rotor fluxes in synchronous direct and quadrature axis reference frame referred to stator, respectively; ω_e is the angular synchronous speed of the motor, $\sigma = 1 - \frac{L_m^2}{L_s L_r}$, $T_r = \frac{L_r}{R_r}$, $\gamma = \frac{R_s}{\sigma L_s} + \frac{1-\sigma}{\sigma T_r}$, $\beta = \frac{Lm}{\sigma L_s L_r}$, and $\zeta = \frac{1}{T_r}$. The motor parameters are listed in Table 1.

To compensate the change in rotor resistance due to prolonged operation, the slip speed (ω_{sl}) in IFOCIM method is used to be [17]:

$$\left.\begin{aligned} \omega_{sl} &= (\omega_e - \omega_r) = \frac{\alpha}{T_r} L_m T_{re} \\ T_{re} &= \left(K_{pw} + K_{iw} \int dt\right)(\omega_{\text{ref}} - \omega_r) \end{aligned}\right\} \tag{6}$$

Journal: Article No.: 1389 TYPESET DISK LE CP Disp.:2021/4/3 Pages: 13 Layout: Small

The direct and quadrature reference currents of the stator can be expressed as the following:

$$\left.\begin{aligned} i_{\text{dref}} &= \frac{\psi_{\text{dref}} + T_r \dot{\psi}_{\text{dref}}}{L_m} - \psi_{qr} T_{re} \\ i_{\text{qref}} &= \psi_{dr} T_{re} \end{aligned}\right\} \tag{7}$$

where α is the gain of the compensator, ψ_{dref} is the rotor reference flux, and $K_{p\omega}$ and $K_{i\omega}$ are the proportional and integral gains of the speed controller, respectively. From Fig. 1, Eqs (1)–(7), and by defining the state variables $x_1 = i_{ds}, x_2 = i_{qs}, x_3 = \psi_{dr}, x_4 = \psi_{qr}, x_5 = \omega_r$, $x_6 = \left(K_{pw} + K_{iw} \int \mathrm{d}t\right)(\omega_{\text{ref}} - \omega_r), x_7 = \int (i_{\text{dref}} - i_{ds})\,\mathrm{d}t$, and $x_8 = \int \left(i_{\text{qref}} - i_{qs}\right)\mathrm{d}t$, the higher-order model (HOM) of IFOCIM system can de expressed by the following equations:

$$\begin{aligned} \dot{x}_1 = &-\gamma x_1 + \left[x_5 + \frac{\alpha}{T_r} L_m x_6\right] x_2 + \frac{\beta}{T_r} x_3 \\ &+ \beta \frac{L_r}{L_m} K pd \left[\frac{1}{L_m}\psi_{\text{dref}} + \frac{T_r}{L_m}\dot{\psi}_{\text{dref}} - x_4 x_6 - x_1\right] \\ &+ \beta x_5 x_4 + \beta \frac{L_r}{L_m} K_{id} x_7 \end{aligned} \tag{8}$$

$$\begin{aligned} \dot{x}_2 = &-\left[x_5 + \frac{\alpha}{T_r} L_m x_6\right] x_1 - \gamma x_2 - \beta x_5 x_3 + \frac{\beta}{T_r} x_4 \\ &+ \beta \frac{L_r}{L_m} K pq \left[x_3 x_6 - x_2\right] + \beta \frac{L_r}{L_m} K_{iq} x_8 \end{aligned} \tag{9}$$

$$\dot{x}_3 = \frac{L_m}{T_r} x_1 - \frac{1}{T_r} x_3 + \frac{\alpha}{T_r} L_m x_4 x_6 \tag{10}$$

$$\dot{x}_4 = \frac{L_m}{T_r} x_2 - \frac{1}{T_r} x_4 - \frac{\alpha}{T_r} L_m x_3 x_6 \tag{11}$$

$$\dot{x}_5 = \frac{P}{2J}\left[K\left(x_2 x_3 - x_1 x_4\right) - T_L\right] - \frac{B_m}{J} x_5 \tag{12}$$

$$\dot{x}_6 = -K_{pw}\left[\frac{P}{2J}\left[K\left(x_2 x_3 - x_1 x_4\right) - T_L\right] - \frac{B_m}{J} x_5\right] + K_{iw}\left(\omega_{\text{ref}} - x_5\right) \tag{13}$$

$$\dot{x}_7 = -x_1 - x_4 x_6 + \frac{1}{Lm}\psi_{\text{dref}} + \frac{T_r}{L_m}\dot{\psi}_{\text{dref}} \tag{14}$$

$$\dot{x}_8 = -x_2 + x_3 x_6 \tag{15}$$

where $K = \frac{3}{2}\frac{P}{2}\frac{L_m}{L_r}$, K_{pd}, K_{id}, K_{pq}, and K_{iq} are the proportional and integral gains for the i_{ds}, i_{qs} controllers, respectively.

3 Dynamical analysis

The IM parameters are listed in Table 2 [15], and the PI controller gains are chosen to be $K_{pd} = K_{pq} = 50$, $K_{id} = K_{iq} = 100$, $K_{p\omega} = 20$, $K_{i\omega} = 5$, $\psi_{\text{dref}} = 0.55$ Wb, and α is selected to be 1.3. The load torque and the speed reference are set to be 3 Nm and 50 rad/sec, respectively.

Journal: Article No.: 1389 TYPESET DISK LE CP Disp.:2021/4/3 Pages: 13 Layout: Small

Table 2 IM parameters for simulation

Parameter	Value	Parameter	Value
P	4	L_r (H)	0.2235
R_s (Ω)	0.76	L_m (H)	0.2176
L_s (H)	0.2248	J (kg m^2)	0.0111
R_r (Ω)	0.675	B_m (Nm/rad/s)	7.355×10^{-4}

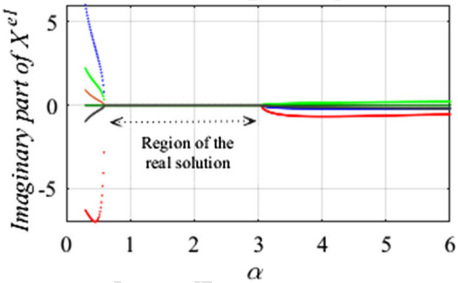

Fig. 2 Locus of real solution of X^{e1} as a function of α. System parameters are $K_{pd} = K_{pq} = 50$, $K_{id} = K_{iq} = 100$, $K_{p\omega} = 20$, $K_{i\omega} = 5$, and $\psi_{\text{dref}} = 0.55$ Wb

3.1 Equilibrium points

Let the notations x_i^e, $i = 1, 2, \ldots, 8$ indicate the equilibrium point states. By considering $x_5^e = \omega_{\text{ref}}$ and solving Eq. (8) to (15), the values of the states at the equilibrium point can be described as:

$$X^e = \begin{bmatrix} x_1^e \\ x_2^e \\ x_3^e \\ x_4^e \\ x_5^e \\ x_6^e \\ x_7^e \\ x_8^e \end{bmatrix} = \begin{bmatrix} \frac{-m \pm \sqrt{m^2 - 4ln}}{2l} \\ \frac{B_m \omega_{\text{ref}} + \frac{P}{2} T_L}{\alpha \frac{P}{2} K \psi_{\text{dref}}} \\ L_m x_1^e (1-\alpha) + \alpha \psi_{\text{dref}} \\ L_m x_2^e (1-\alpha) \\ \omega_{\text{ref}} \\ \frac{x_2^e}{x_3^e} \\ \frac{L_m}{\beta L_r K_{id}} \left(a_1 x_1^e + a_2 \frac{(x_2^e)^2}{x_3^e} - a_3 \right) \\ \frac{L_m}{\beta L_r K_{iq}} \left(\left(b_1 + b_2 \frac{x_2^e}{x_3^e} \right) x_1^e + b_3 \right) \end{bmatrix} \tag{16}$$

where $l = (1-\alpha) L_m^2$, $m = (2\alpha - 1) L_m \psi_{\text{dref}}$, $n = \frac{l \left(B_m \omega_{\text{ref}} + \frac{P}{2} T_L \right)^2}{\left(\alpha \frac{P}{2} K \psi_{\text{dref}} \right)^2} - \alpha \psi_{\text{dref}}^2$, $a_1 = \gamma - \beta \frac{L_m}{T_r} (1-\alpha) + \frac{\beta L_r}{L_m} K_{pd}$, $a_2 = \beta L_r (1-\alpha) K_{pd} - \alpha \frac{L_m}{T_r}$, $a_3 = (\beta L_m (1-\alpha) + 1)\, \omega_{\text{ref}} \frac{B_m \omega_{\text{ref}} + \frac{P}{2} T_L}{\alpha \frac{P}{2} K \psi_{\text{dref}}} + \left(\frac{\alpha \beta}{T_r} + \frac{\beta L_r K_{pd}}{L_m^2} \right) \psi_{\text{dref}}$, $b_1 = \omega_{\text{ref}} + \beta \omega_{\text{ref}} L_m (1-\alpha)$, $b_2 = \frac{\alpha L_m}{T_r}$, and $b_3 = \left(\gamma - \frac{\beta L_m}{T_r} (1-\alpha) \right) \frac{B_m \omega_{\text{ref}} + \frac{P}{2} T_L}{\alpha \frac{P}{2} K \psi_{\text{dref}}} + \alpha \beta \omega_{\text{ref}} \psi_{\text{dref}}$.

Journal: Article No.: 1389 TYPESET DISK LE CP Disp.:2021/4/3 Pages: 13 Layout: Small

From Eq. (16), X^e is not unique for $\alpha \neq 1$, otherwise X^e has unique solution. The real solution of X^e is obtained when:

$$\frac{2L_m\left(B_m\omega_{\text{ref}}+\frac{P}{2}T_L\right)}{2L_m\left(B_m\omega_{\text{ref}}+\frac{P}{2}T_L\right)+\frac{P}{2}K\psi_{\text{dref}}^2} \le \alpha \le \frac{2L_m\left(B_m\omega_{\text{ref}}+\frac{P}{2}T_L\right)}{2L_m\left(B_m\omega_{\text{ref}}+\frac{P}{2}T_L\right)-\frac{P}{2}K\psi_{\text{dref}}^2} \tag{17}$$

According to Eq. (17) and Fig. 2, the real solution is obtained in the range of $0.61 \le \alpha \le 3.04$. In the outside of this range of α, the system does not have real equilibrium points.

3.2 Stability of equilibrium points

The IM parameters as in Table 2 [15] and PI controller gains are chosen to be $K_{pd} = K_{pq} = 50$, $K_{id} = K_{iq} = 100$, $K_{p\omega} = 20$, $0 \le K_{i\omega} \le 120$, $\psi_{\text{dref}} = 0.55$ Wb, and α=1.3. According to Eq. (16), the system has two different equilibrium points:
$X^{e1} = (2.783, 1.446, 0.533, -0.094, 50, 2.71, 0.12, -0.531)^T$
$X^{e2} = (10.697, 1.446, 0.017, -0.094, 50, 86.561, 0.344, -0.13)^T$
Based on the linearization theorem, the differential system is described in matrix form close to the equilibrium point as the following:

$$\dot{X} = J(x)\,X \tag{18}$$

where J(x) is the Jacobian matrix of the system, $X = (x_1, x_2, x_3, x_4, x_5, x_6, x_7, x_8)^T$ is the vector of the system variables, and $\dot{X} = (\dot{x}_1, \dot{x}_2, \dot{x}_3, \dot{x}_4, \dot{x}_5, \dot{x}_6, \dot{x}_7, \dot{x}_8)^T$

The Jacobian matrix of the linearized model can be given as:

$$J(x) = \begin{bmatrix} J_{6\times6} & J_{6\times2} \\ J_{2\times6} & 0_{2\times2} \end{bmatrix} \tag{19}$$

where

$$J_{6\times6} = \begin{bmatrix} -\gamma - c_1K_{pd} & x_5 + c_2x_6 & \frac{\beta}{T_r} & \beta x_5 - c_1K_{pd}x_6 & -x_2 - \beta x_4 & c_2x_2 - c_1K_{pd}x_4 \\ -x_5 - c_2x_6 & -\gamma - c_1K_{pq} & c_1K_{pq}x_6 - \beta x_5 & \frac{\beta}{T_r} & x_1 + \beta x_3 & -c_2x_1 + c_1K_{pq}x_3 \\ \frac{c_2}{\alpha} & 0 & \frac{-1}{T_r} & c_2x_6 & 0 & c_2x_4 \\ 0 & \frac{c_2}{\alpha} & -c_2x_6 & \frac{-1}{T_r} & 0 & -c_2x_3 \\ c_4x_4 & -c_4x_3 & -c_4x_2 & c_4x_1 & -c_3 & 0 \\ c_4K_{pw}x_4 & -c_4K_{pw}x_3 & -c_4K_{pw}x_2 & c_4K_{pw}x_1 & K_{iw} - c_3K_{pw} & 0 \end{bmatrix},$$

$$J_{6\times2} = \begin{bmatrix} c_1K_{id} & 0 & 0 & 0 & 0 & 0 \\ 0 & c_1K_{iq} & 0 & 0 & 0 & 0 \end{bmatrix}^T, \quad J_{2\times6} = \begin{bmatrix} -1 & 0 & 0 & -x_6 & 0 & -x_4 \\ 0 & -1 & x_6 & 0 & 0 & x_3 \end{bmatrix},$$

$c_1 = \beta\frac{L_r}{L_m}$, $c_2 = \alpha\frac{L_m}{T_r}$, $c_3 = \frac{B_m}{J}$, and $c_4 = \frac{1.5L_mP^2}{4JL_r}$

The eigenvalues of the Jacobian matrix described in Eq.(19) are checked numerically. The equilibrium point X^{e1} is stable, while X^{e2} is unstable for $K_{i\omega} > 106.4$. For $K_{i\omega} = 106.4$, the eigenvalues are listed in Table 3.

3.3 Bifurcation diagram

The system specified by Eqs. (8)–(15) has been simulated numerically for different values of the controller parameters. The bifurcation diagram and corresponding Lyapunov exponents (LEs) spectrum as a function of parameter α are shown in Fig. 3. The parameters are $K_{pd} = K_{pq} = 50$, $K_{id} = K_{iq} = 100$, $K_{p\omega} = 20$, and $\psi_{\text{dref}} = 0.55$ Wb. From Fig. 3, one can note that, for a certain value of controller gains with varying of α, the system bifurcates into period-1, period-2, period-4 and chaotic attractor. For $K_{i\omega} = 5$ and α is varied from

Journal: Article No.: 1389 TYPESET DISK LE CP Disp.:2021/4/3 Pages: 13 Layout: Small

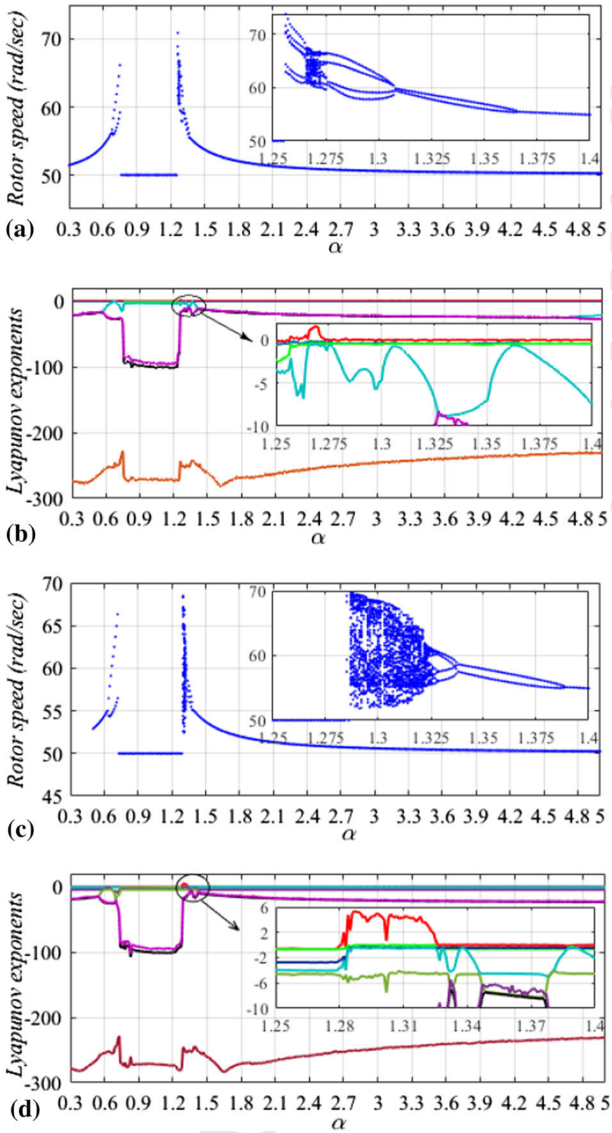

Fig. 3 Speed bifurcation diagram and Lyapunov exponents due to α change at $K_{pd} = K_{pq} = 50$, $K_{id} = K_{iq} = 100$, and $K_{p\omega} = 20$ **a** bifurcation diagram for $K_{i\omega} = 5$, **b** corresponding Lyapunov exponents, **c** bifurcation diagram for $K_{i\omega} = 90$ and **d** corresponding Lyapunov exponents

0.3 to 5, Fig. 3a depicts that the dominant cases are period-1, period-2, and period-4, in the ranges of α from 0.3 to 0.671, 1.256 to 1.265, and 1.273 to 5 and the fixed point is seen in the range from 0.672 to 1.255. Hopf bifurcation occurs at $\alpha = 1.256$ where the chaos behavior is noted during tiny range from 1.266 to 1.272 only. Figure 3b confirms the system behavior shown in Fig. 3a, where the largest LEs are zero for the periodic solution in the ranges $0.3 \leq \alpha \leq 0, 671$, $1, 256 \leq \alpha \leq 1.265$, and $1.273 \leq \alpha \leq 5$, all LEs are negative for the range of $0.672 \leq \alpha \leq 1.255$, while one of LEs became positive for $1.266 \leq \alpha \leq 1.272$.

Journal: Article No.: 1389 TYPESET DISK LE CP Disp.:2021/4/3 Pages: 13 Layout: Small

Table 3 The eigenvalues of the linearized system for $K_{pd} = K_{pq} = 50$, $K_{id} = K_{iq} = 100$, $K_{p\omega} = 20$, $K_{i\omega} = 106.4$, $\psi_{\mathrm{dref}} = 0.55$ Wb, $\alpha = 1.3$, $T_l = 3$ Nm and $\omega_{\mathrm{ref}} = 50$ rad/s,

Eigenvalues	X^{e1}	X^{e2}
λ_1	-7832.1	$-7785.7 + 175.27i$
λ_2	$-3913.8 + 2913.86i$	$-7785.7 - 175.27i$
λ_3	$-3913.8 - 2913.86i$	-71.9
λ_4	$-0.487 + 0.064i$	-38.644
λ_5	$-0.487 - 0.064i$	14.707
λ_6	-2.81	-5.125
λ_7	-4.174	$-0.468 + 0.047i$
λ_8	-5.322	$-0.468 - 0.047i$

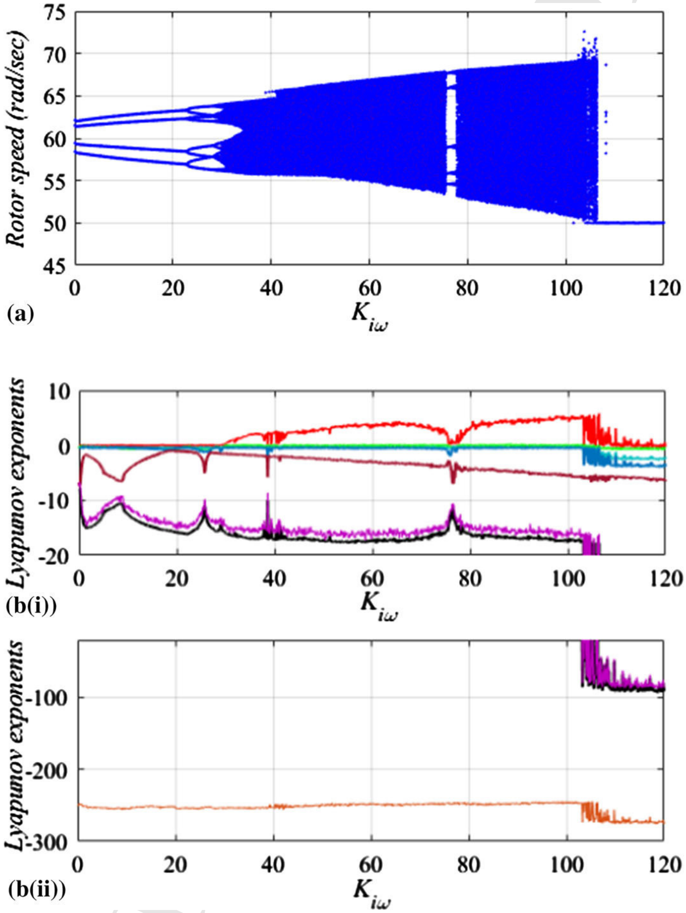

Fig. 4 IFOCIM drive system with $K_{pd} = K_{pq} = 50$, $K_{id} = K_{iq} = 100$, $K_{p\omega} = 20$, $\psi_{\mathrm{dref}} = 0.55$ Wb, $\alpha = 1.3$, $\omega_{\mathrm{ref}} = 50$ and $T_L = 3$ Nm: **a** bifurcation diagram and the corresponding spectrum of the seven Lyapunov exponents **b**(i) L_1, L_2, L_3, L_4,L_5, L_6, L_7 and the eighth Lyapunov exponent **b**(ii) L_8 illustrate various behaviors of system with variation of $K_{i\omega}$ upward in the range $0 \leq K_{i\omega} \leq 120$

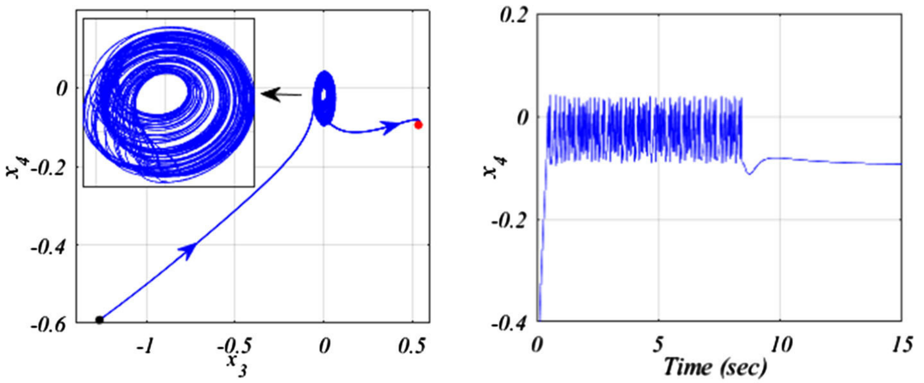

(a) Phase portrait. **(b)** Time response.

Fig. 5 Transient chaotic behavior with system parameters $K_{pd} = K_{pq} = 50$, $K_{id} = K_{iq} = 100$, $K_{p\omega} = 20$, $K_{i\omega} = 110$, $\psi_{\text{dref}} = 0.55$ Wb, $\alpha = 1.3$, $\omega_{\text{ref}} = 50$ and $T_L = 3$ Nm: **a** phase portrait projection (x_3, x_4) and the initial value $(x_1(0), x_2(0), x_3(0), x_4(0), x_5(0), x_6(0), x_7(0), x_8(0))$=(0,0,-1.265,-0.5918,0,0,0,0) and **b** the corresponding time series of x_4

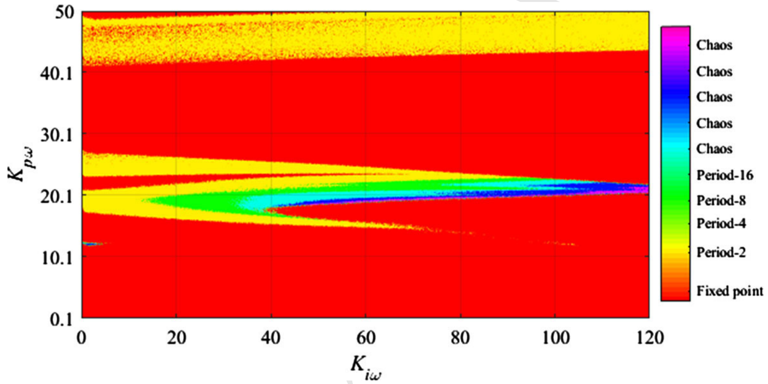

Fig. 6 Two-dimensional speed bifurcation diagram where the system parameters are $K_{pd} = K_{pq} = 50$, $K_{id} = K_{iq} = 100$, $\psi_{\text{dref}} = 0.55$ Wb, $\alpha = 1.3$, $T_L = 3$ Nm and $\omega_{\text{ref}} = 50$ rad/s

For $K_{i\omega} = 90$, Fig. 3c, d shows that the boundaries of the bifurcation regions are shifted and the chaotic domain is increased. The results show that the chaos occurs in a very small range of α, while it is noted that the results in the previous studies [9–14, 16] showed that the general behavior of the system is the occurrence of SNB, HB, BTB, and ZHB.

As shown in Fig. 3, the value of α which leads to chaos is varied in a small ranges around 1.27 for $K_{i\omega} = 5$ and around 1.3 for $K_{i\omega} = 90$. Besides, in practical application upper limit value of α is about 1.5 [18]. Therefore, $\alpha = 1.3$ is selected to investigate the system dynamics due to the changes of the controller gain(s).

The system dynamics is verified numerically to investigate the bifurcation behavior due to $K_{i\omega}$ change for a certain value of $\alpha (= 1.3)$ as illustrated in Fig. 4a. It is noted that for $K_{i\omega} = 0$, a stable periodic solution occurs with period-2; period-doubling bifurcation route to chaos is appeared for $K_{i\omega} \geq 0.1$. The period-4 occurs for $K_{i\omega}$ from 0.1 to 23, period-8 for $K_{i\omega}$ from 23.1 to 28.3, and period-16 for $K_{i\omega}$ from 28.4 to 29.7. The system exhibits chaotic for $K_{i\omega}$ from 29.8 to 106.3, while period-5 and period-10 are also noted at a windows

Journal: Article No.: **1389** TYPESET DISK LE CP Disp.:**2021/4/3** Pages: **13** Layout: **Small**

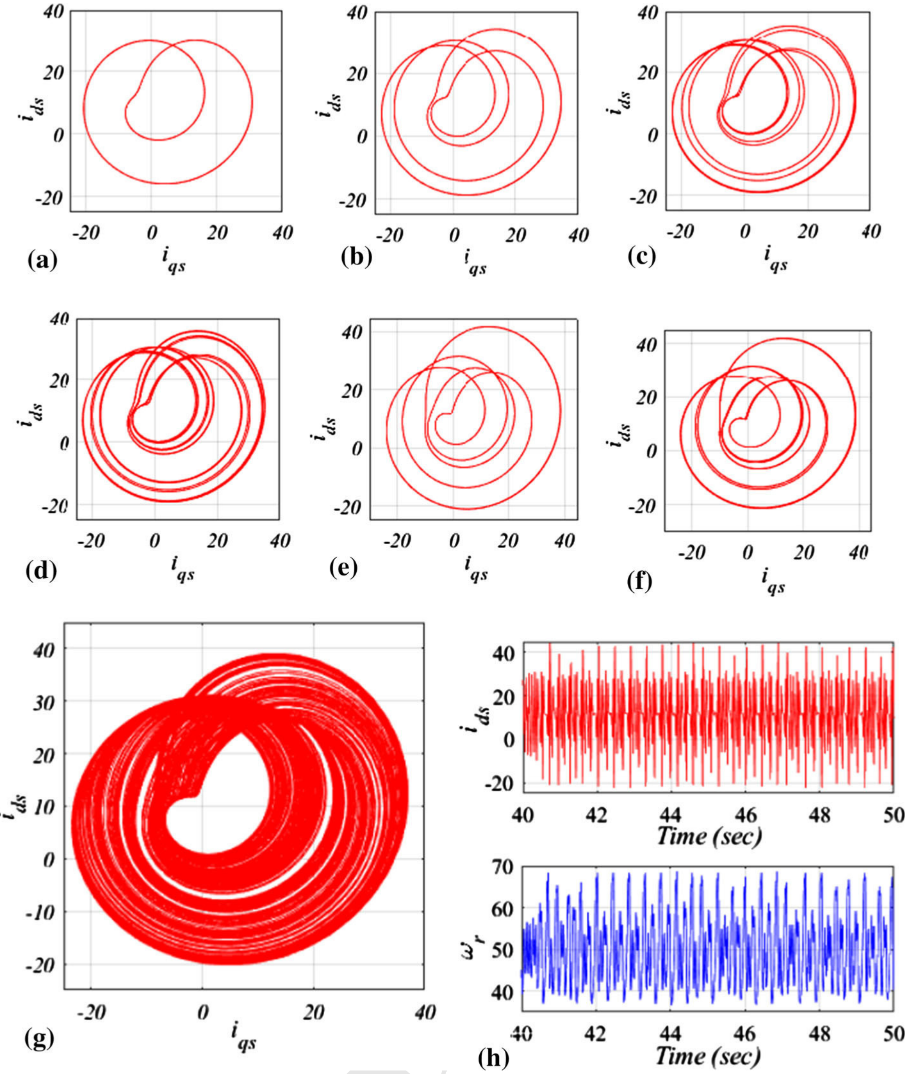

Fig. 7 Phase portrait projected (i_{qs}, i_{ds}) in A with system parameters that are $K_{pd} = K_{pq} = 50$, $K_{id} = K_{iq} = 100$, $K_{p\omega} = 20$, $\psi_{\text{dref}} = 0.55$ Wb, $\alpha = 1.3$; $T_L = 3$ Nm and $\omega_{\text{ref}} = 50$ rad/sec **a** for $K_{i\omega} = 0$, **b** for $K_{i\omega} = 20$, **c** for $K_{i\omega} = 26$, **d** for $K_{i\omega} = 29$, **e** for $K_{i\omega} = 76$, **f** for $K_{i\omega} = 77$, **g** for $K_{i\omega} = 50$, and **h** time series responses for direct currents (i_{ds}) in A and rotor speed (ω_r) in rad/sec for $K_{i\omega} = 50$

$K_{i\omega}$ from 75.6 to 76.7 and $K_{i\omega}$ from 76.8 to 77.7. Also, there are windows for fixed-point spread between the chaos region for $K_{i\omega}$ from 104.3 to 104.6 and $K_{i\omega}$ from 104.9 to 105. For $K_{i\omega} \geq 106.4$; the system tracks speed command perfectly which is noted as fixed point.

The Lyapunov exponents spectrum is obtained with respect to $K_{i\omega}$ change. The simulation results confirmed the bifurcation diagram. From Fig. 4b, the largest Lyapunov exponents spectrum shows that the system has periodic behavior for $K_{i\omega}$ from 0 to 29.7 and then the chaos state has occurred for $K_{i\omega}$ from 29.8 to 106.3. All the eight Lyapunov exponents are negative for $K_{i\omega} \geq 106.4$ which denote fixed-point state. From Fig. 4b, the system shows positive LE

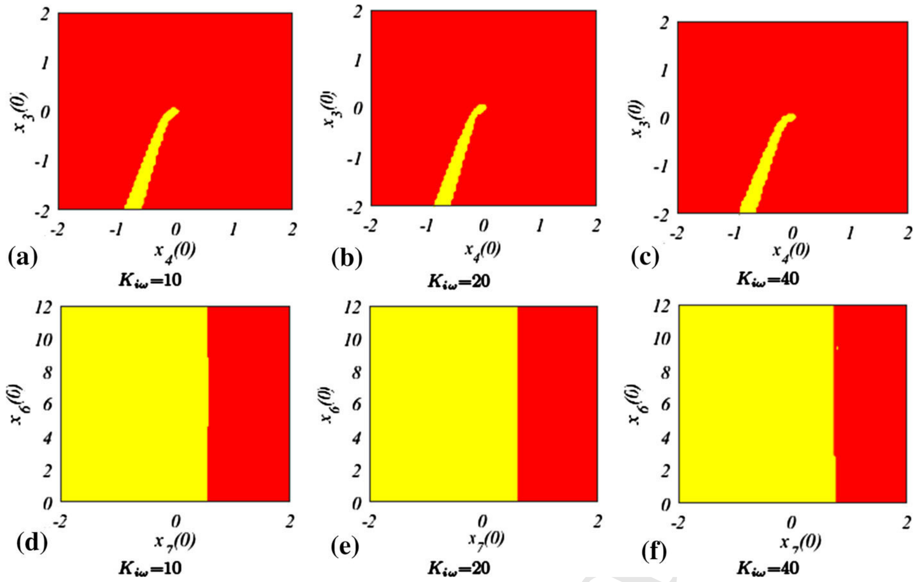

Fig. 8 Basins of attractions with system parameters as in Fig. 4 with $K_{p\omega} = 45$ and $K_{i\omega}$ as mentioned in subfigures, where in **a**, **b**, and **c** x_3 and x_4 are varied with $x_1(0) = 0, x_2(0) = 0, x_5(0) = 0, x_6(0) = 0, x_7(0) = 0$, and $x_8(0) = 0$, **d**, **e**, and **f** x_6 and x_7 are varied with $x_1(0) = 0, x_2(0) = 0, x_3(0) = 0, x_4(0) = 0, x_5(0) = 0$, and $x_8(0) = 0$, fixed-point behavior (red) and periodic behavior (yellow)

in the fixed-point behavior region that means it has transient chaotic behavior followed by fixed-point steady-state response. Figure 5 states the system transient chaos, Fig. 5a illustrates the phase portrait for initial value $(x_1(0), x_2(0), x_3(0), x_4(0), x_5(0), x_6(0), x_7(0), x_8(0)) =$ (0,0,-1.265,-0.5918,0,0,0,0), and Fig. 5b shows the corresponding time series.

The effect of change of speed controller gains ($K_{p\omega}$ and $K_{i\omega}$) has been investigated to get the two-dimensional bifurcation diagram as shown in Fig. 6. The red zones denote the fixed-point behavior, while the yellow, light green, and green zones denote quasi-periodic behavior. The chaos zones are colored with light blue, blue, light purple, and purple. The diversity of the colors is due to the strength of the chaotic behavior. It is noted that the fixed-point state has the largest area of the 2D diagram, while the chaos behavior has very small area. The diagram simplifies the boundaries of each of $K_{p\omega}$ and $K_{i\omega}$ for the designer to be used according to the application.

Figure 7 shows the phase portrait projected (i_{qs}, i_{ds}) and the corresponding time response with $K_{pd} = K_{pq} = 50$, $K_{id} = K_{iq} = 100$, $K_{p\omega} = 20$, $\psi_{\text{dref}} = 0.55$ Wb, $\alpha = 1.3$; $T_L = 3$ Nm and $\omega_{\text{ref}} = 50$. Figure 7a illustrates period-2 when $K_{i\omega} = 0$. Period-doubling period-4, period-8, and period-16 are plotted at $K_{i\omega} = 20$, 26, and 29 as shown in Fig. 7b–d, respectively. Period doubling from period-5 to period-10 is illustrated in Fig. 7e, f when $K_{i\omega}$ equals 76 and 77, respectively. Chaotic behavior is represented in Fig. 7g at $K_{i\omega} = 50$, while Fig. 7h represents the time series responses for direct currents (i_{ds}) and rotor speed (ω_r) at $K_{i\omega} = 50$. The figures emphasize the bifurcation diagrams and Lyapunov exponents spectrum.

Journal: Article No.: 1389 TYPESET DISK LE CP Disp.:2021/4/3 Pages: 13 Layout: Small

3.4 Basins of attractions

This subsection discusses the basins of attractions and multistability. The nonlinear systems are sensitive to the changes in its parameters and the initial conditions of the state variables. Some of the system variables' initial values have been used to discover the IFOC drive system behavior. In Fig. 8, the system shows two different attractors: fixed point (red) and periodic (yellow). Figure 8a–c represents different attractors with respect to the change in initial values of x_3 and x_4 with $K_{iw} = 10$, 20, and 40, respectively. The other variables have constant initial values $x_1(0) = 0$, $x_2(0) = 0$, $x_5(0) = 0$, $x_6(0) = 0$, $x_7(0) = 0$, and $x_8(0) = 0$. As shown in Fig. 8d–f, the initial values of x_1, x_2, x_3, x_4, x_5, and x_8 have been adjusted to be 0, 0, 0, 0, 0, and 0 for $K_{iw} = 10$, 20, and 40, respectively, and the values of $x_6(0)$, $x_7(0)$ are changed. Figure 8d–f displays fixed point and periodic attractors due to the changes in the initial values of x_6 and x_7 for $K_{iw} = 20$. These different attractors, which are shown in Fig. 1, reveal that the IFOCIM system is sensitive to the variation of the initial value of IFOC system variables.

From Figs. 4, 5, and 8, one can conclude that the IFOCIM model has multistability.

4 Conclusions

The full-order three-phase IM has been modeled in synchronous reference frame and controlled by using indirect field-oriented control method. The numerical analysis is used to investigate the system behavior due to control parameters change. The variation of slip speed compensator gain, integral gain, and proportional gain of speed loop controller are used to test the system dynamics. The simulation results show interesting notes related to the gain of the slip speed compensator bifurcation values where the chaos behavior is shown in very small region which is difficult to be indicated compared with the dominant limit cycles solutions; while the quasi-periodic behavior has the largest region, the fixed-point state has been noted in significant range of α. Also, the results show that the system has been bifurcated into period-2, period-4, period-8, period-16, and then the system becomes chaotic due to integral gain variation of speed loop. The bifurcation diagram and Lyapunov exponent spectrum confirm these situations. Period-5 and period-10 have been indicated in a window inside the bifurcation diagram. The 2D bifurcation diagram gives visualization about the accepted ranges for each of $K_{p\omega}$ and $K_{i\omega}$ to avoid the undesirable cases. Also, the system has multistability for different initial values of the state variables. In future work, a suitable control method will be used to suppress the chaos in the IFOC drive system.

References

1. F. Lin, C. Liaw, I.E.E.E. Int, Symp. Ind. Electron. **40**, 658 (1992)
2. T. Matsuo, T. Lipo, P.E.S.C. Rec, IEEE Annu. Power Electron. Spec. Conf. **1**, 425 (1993)
3. B. Bose, *Modern Power Electronics and AC Drives* (Prentice Hall PTR, New York, 2001).
4. H. Khalil, E. Strangas, S. Jurkovic, IEEE Trans. Control Syst. Technol. **17**, 327 (2009)
5. D. Holmes, B. McGrath, S. Parker, IEEE Trans. Ind. Electron. **59**, 3680 (2012)
6. P. Alkorta, O. Barambones, J. Cortajarena et al., IEEE Trans. Ind. Electron. **61**, 5126 (2014)
7. R. Krishnan, A. Bharadwaj, IEEE Trans. Power Electron. **6**, 695 (1991)
8. L. Zhao, J. Huang, J. Chen et al., IEEE Trans. Power Electron. **31**, 6494 (2016)
9. A. Bazanella, R. Reginatto, IEEE Trans. Automat. Control **45**, 1226 (2000)
10. A. Bazanella, R. Reginatto, Automatica **37**, 1811 (2001)
11. F. Gordillo, F. Salas, R. Ortega, Automatica **38**, 829 (2002)
12. F. Salas, F. Gordillo, J. Aracil, et al., 43rd IEEE Conference on Decision and Control (2004)

Journal: Article No.: **1389** ☐ TYPESET ☐ DISK ☐ LE ☐ CP Disp.:**2021/4/3** Pages: **13** Layout: **Small**

13. F. Salas, F. Gordillo, J. Aracil et al., Int. J. Bifurc. Chaos **18**, 779 (2008)
14. Y. Lu, H. Li, W. Li, IEEE Conf. Ind. Electron. Appl. ICIEA **5**, 3438 (2009)
15. Y. Gao, K.T. Chau, IEEE Power Electron. Spec. Conf. **31**, 1083 (2003)
16. J. Jain, S. Ghosh, S. Maity, IEEE Trans. Control Syst. Technol. **6**, 282 (2018)
17. K.T. Chua, Z. Wang, *Chaos in Electric Drive Systems: Analysis, Control and Application* (Wiley, Singapore, 2011).
18. R. Krishnan, F. Doran, IEEE Trans. Ind. Appl. **4**, 623 (1987)

Journal: Article No.: 1389 TYPESET DISK LE CP Disp.:2021/4/3 Pages: 13 Layout: Small

Journal: 13360
Article: 1389

Author Query Form

Please ensure you fill out your response to the queries raised below and return this form along with your corrections

Dear Author

During the process of typesetting your article, the following queries have arisen. Please check your typeset proof carefully against the queries listed below and mark the necessary changes either directly on the proof/online grid or in the 'Author's response' area provided below

Query	Details required	Author's response
1.	Please confirm if the author names are presented accurately and in the correct sequence (given name, middle name/initial, family name). Author 1 Given name: [Ahmed Sadeq], Last name: [Hunaish], Author 2 Given name: [Fadhil Rahma], Last name: [Tahir]. Also, kindly confirm the details in the metadata are correct.	
2.	Please confirm if the corresponding author is correctly identified.	
3.	Please check the edit made in the article title.	